This article has been accepted for inclusion in a future issue of this journal. Content is final as presented, with the exception of pagination.

A High-Current-Density Terahertz Electron-Optical System Based on Carbon Nanotube Cold Cathode

Yunlong Gu, Xuesong Yuan, Xiaotao Xu, Matthew Cole, *Senior Member, IEEE*, Qingyun Chen, Yu Zhang, Bin Wang, *Member, IEEE*, Hailong Li, *Member, IEEE*, Yong Yin, *Member, IEEE*, and Yang Yan

***Abstract*— A high-current-density terahertz electron-optical system based on a carbon nanotube (CNT) cold cathode has been investigated in order to solve notable mode competition in high-order harmonic gyrotrons. Simulation results show that a near-axis electron beam can be generated, with a beam current of 160 mA at an accelerating voltage of 23.5 kV. The source supports the electron beam with a velocity ratio of 1.1 and a guiding center radius of 57 μm. A narrow beam spatial distribution is evidenced by adjusting control anode voltage, satisfying the need for high operating current density in slow wave devices. The current density of the electron beam is up to 620 A/cm^2 at the output port and the velocity ratio is 0.44, with parallel energy accounting for 84% of the total energy.**

***Index Terms*— Carbon nanotube (CNT), cold cathode, gyrotron, high-current-density, high-order harmonic, mode competition, terahertz.**

I. Introduction

DRIVING the rapid development of terahertz science and technology, terahertz radiation sources have found wide use in radar, communications, and biomedical applications [1], [2]. Compared with the solid-state sources, vacuum electron radiation sources (VERSs) offer advantageously high output powers (up to 1 GW) and high operating frequencies (up to 1 THz), making them well-suited to the demanding requirements of industry and commerce [3]. Gyrotron structures, fast-wave devices with some of the highest recorded output powers, have received extensive attention in space communication, thermonuclear fusion, and medical diagnosis [4]–[11]. In such devices, affordable and movable scale superconducting magnets can generate magnetic fields of 10–15 T, which corresponds to electron-cyclotron frequencies of 0.3–0.4 THz [12]. Nevertheless, such superconducting magnets remain bulky and account for significant volumes within present designs. Reducing the magnet size deleteriously reduces the attainable magnetic field, and in doing so compromises the device functionality. However, the required magnetic field, and hence, magnet dimensions, can be greatly decreased by engineering high-order harmonic operation. Nevertheless, mode competition hinders the development of gyrotrons when operating at high-order harmonic. A third-harmonic gyrotron with axis-encircling electron beam (large-orbit gyrotron), operating at 1 THz, has recently been developed [13]. One solution to mode competition is decreasing the electron beam radius. As the radius of the electron beam becomes increasingly small, there is significant mode depletion, resulting in only the TE_{25} mode to participate in mode competition. However, the design of such electron-optical system is relatively complex, requires fine machining, accurate modeling, and careful assembly, especially within the magnetic field system [14].

By increasing the operating frequency (up to terahertz frequency band), the minimum working current density of traditional terahertz VERS systems increases dramatically, typically to hundreds of A/cm^2. The minimum current density for some electron tubes, such as Ledatrons, traveling wave tubes (TWTs), Reflex Klystrons, and backward wave oscillators (BWOs), is 330, 70, 216, and 874 A/cm^2, respectively [15]–[17]. Despite significant research efforts, such large minimum current densities continue to plague the development of traditional VERS systems. Due to their cost, ease of access, and technological maturity, almost all commercial VERS continue to employ thermionic cathodes as the electron emission sources. Nevertheless, thermionic cathodes suffer from significant functional limitations, such as the need for high operating temperatures which limits system design opportunities due to thermal dissipation challenges, large operating volume, and comparatively slow response times [18]–[20]. Conversely, field

Manuscript received June 18, 2020; revised September 12, 2020; accepted October 13, 2020. This work was supported in part by the National Key Research and Development Program of China under Grant 2019YFA0210202, in part by the National Natural Science Foundation of China under Grant 61771096, and in part by the Fundamental Research Funds for the Central Universities under Grant ZYGX2019J012 and Grant ZYGX2019Z006. The review of this article was arranged by Editor L. Kumar. *(Corresponding author: Xuesong Yuan.)*

Yunlong Gu, Xuesong Yuan, Xiaotao Xu, Qingyun Chen, Bin Wang, Hailong Li, Yong Yin, and Yang Yan are with the Terahertz Science and Technology Key Laboratory of Sichuan Province, School of Electronic Science and Engineering, University of Electronic Science and Technology of China, Chengdu 610054, China (e-mail: yuanxs@uestc.edu.cn).

Matthew Cole is with the Department of Electronic and Electrical Engineering, University of Bath, Bath BA2 7AY, U.K. (e-mail: m.t.cole@bath.ac.uk).

Yu Zhang is with the State Key Laboratory Optoelectronic Materials and Technologies, Sun Yat-sen University, Guangzhou 510275, China (e-mail: stszhyu@mail.sysu.edu.cn).

Color versions of one or more of the figures in this article are available online at http://ieeexplore.ieee.org.

Digital Object Identifier 10.1109/TED.2020.3031871

electron emission cold cathodes support almost instantaneous turn-on, the ability to create ultracompact designs, tolerance toward small working volumes which relaxes system evacuation requirements, and the ability to operate at near-room-temperature. As a result, field electron emission cold cathodes are coming to the fore as a leading alternative electron emission technology in a new generation of VERS [21], [22]. Supported by the emergence of new types of 1-D and 2-D nanomaterials, field electron emission systems based on carbon nanotubes (CNTs) have been widely demonstrated to provide high emission current densities, excellent chemical, thermal and temporal stability, and low opening fields, making them a prime candidate for use in a variety of electron emission systems, including display devices, microwave sources, and X-ray tubes [23]–[29].

In this article, a high-current-density terahertz electron-optical system based on CNTs is theoretically and experimentally investigated. Here, we demonstrate the potential of CNT-based field emission sources as a candidate technology for both fast wave devices, such as gyrotrons, as well as slow wave devices, such as TWTs, Klystrons, and BWOs. In this work, a near-axis small orbit electron beam has been obtained. We show that mode competition can be solved using such a system, which offers a guiding center radius of only 57 μm at the 0.6-THz third harmonic TE_{37} mode gyrotron. Meanwhile, design sensitivity to the control anode voltage and magnetic field spatially localized to the cathode have been investigated, with beam current density of 620 A/cm^2 at the output port having been achieved, satisfying the demands of state-of-the-art slow wave devices.

II. Design and Simulation

In this section, we describe the design of the electron-optical system based on a CNT cold cathode. This section explores the cathode, control anode, and accelerating anode. Particle in cell (PIC) simulation has been used throughout to investigate the electron-optical system. Efforts have focused on explicating design sensitivity to control anode voltage and magnetic field in the immediate emission volume. Simulations are based on direct experimental findings from CNT's cold cathodes. To form the electron emitter, CNTs were synthesized on a 0.1-mm diameter Ni80Cr20 alloy wire substrates, outlined in [30]. The experimental results demonstrate a maximum operating emission current density of 7.65 A/cm^2 at 2.13 kV/mm, indicating the CNT's suitability to operate as the emission source in high-current-density terahertz electron-optical systems. To obtain the field emission parameters required for the present technology, dual Ni80Cr20 alloy wires were joined to form a ring emitter, which was subsequently embedded within a rectangular groove within the system. A scanning electron microscope (SEM) image of the coated Ni80Cr20 wire, and the synthesized CNT thin film are shown in Fig. 1 with a Computer Aided Design (CAD) rendering of the toroidal electron emission subsystem.

In order to obtain the field emission parameters of the CNT cold cathode, the emission current density is fit to established empirical data using the simplified Fowler–Nordheim (FN) equation

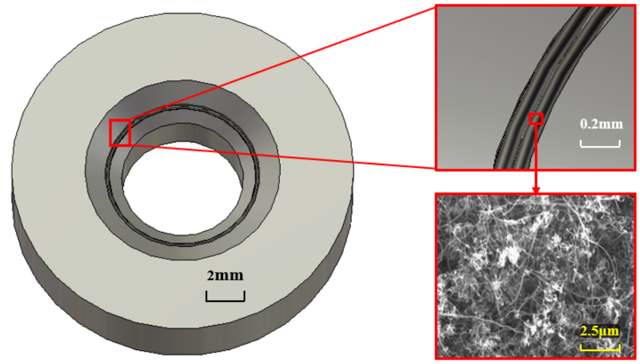

Fig. 1. Simulation structure of dual joined Ni80Cr20 alloy wires. Inset: detailed view of dual Ni80Cr20 alloy wires and areal-view SEM image of the CNT thin film adapted from [30].

$$J = A'E^2\exp\left(-B'/E\right) \quad (1)$$

where A' and B' are the field emission coefficients, $A' = 2.17 \times 10^{-4}\mathrm{A/V^2}$ and $B' = 2.02 \times 10^7$ V/m have been determined by numerical fitting on the basis of our experimental data in [30] and [31]. For the 0.1-mm Ni80Cr20 alloy wire, we find that the simulation mesh must be set to at least 0.01 mm in order to obtain accurate and empirically representative results. This mesh size is far smaller than the electron-optical system (8 mm $\times$ 310 mm), which makes it difficult to directly integrate the alloy wires in a comparatively large volume. In our simulations, as a result, we approximate the dual Ni80Cr20 alloy wires as an equivalent red annular surface emitting band with a width of 0.2 mm, as shown in the inset of Fig. 2(a). Meshes have been investigated using 3-D and 2.5-D PIC simulation software to analyze the computationally demanding spatial and temporal evolution of the electron beam. The field emission coefficient of the simulation model with annular surface emitting band A'' and B'' was numerically fit according to the simulation data of dual Ni80Cr20 alloy wires, where $A'' = 2.15 \times 10^{-4}\mathrm{A/V^2}$ and $B'' = 2.03 \times 10^7$ V/m.

The annular surface emitting band simulations (3-D and 2.5-D) and dual Ni80Cr20 alloy wires (3-D) and its fitting are shown in Fig. 2(a). The coefficient of determination (R_e^2) between 3-D J–E simulation data (dual Ni80Cr20 alloy wires) and 2.5-D J–E simulation data (annular surface emitting band) is 0.9981. Empirical data and equivalent 3-D and 2.5-D models align well.

In order to analyze the velocity and spatial distribution spread of electron beam, the dual-plate electron-optical system has been adopted. The dual Ni80Cr20 alloy wires embedded within a rectangular groove model and annular surface emitting band model are simulated by 2.5-D simulation software, respectively. Simulation results are shown in Fig. 2(b) and (c). Comparing some design parameters of the magnetron injection electron gun, the accelerating voltage is 23.5 kV and the distance between the two flats is 11.4 mm. The electric field on the surface of the emitter is about 2.06 kV/mm. The coefficient of determination (R_s^2) of two groups of the spatial distribution

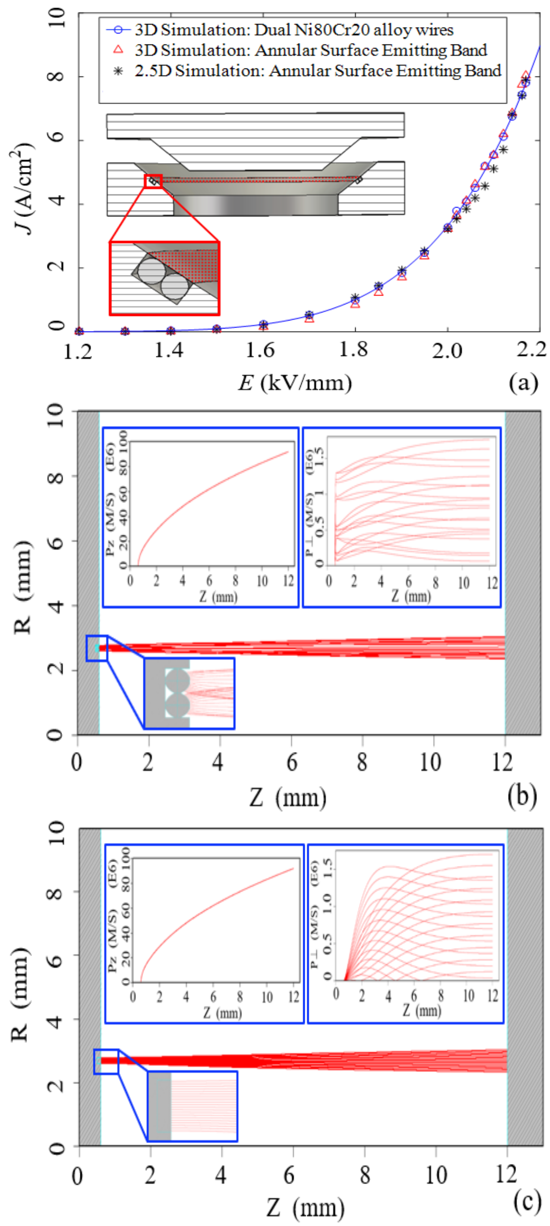

Fig. 2. (a) Simulation emission current density as a function of applied electric field. Inset: detailed view of equivalent simulation structure of dual alloy wires. (b) Electron beam trajectory as a function of axial distance. Inset: parallel and perpendicular momentum as a function of axial distance, detailed view of dual alloy wires embedded within a rectangular groove. (c) Electron beam trajectory as a function of axial distance. Inset: parallel and perpendicular momentum as a function of axial distance, detailed view of annular surface emitting band.

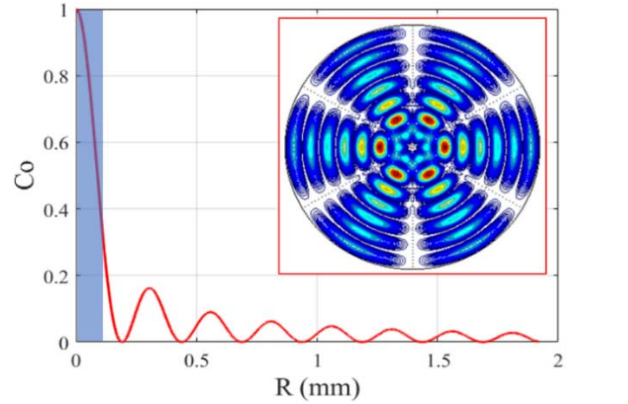

Fig. 3. Normalized beam-wave coupling coefficient as a function of beam radius (the abscissa of the shaded region represents the radius of the electron beam of the electron-optical system, which ranges from 3 to 110 μm). Inset: diagram of TE_{37} mode.

data in the perpendicular direction at the anode ($z = 12$ mm) is 0.9989. The coefficient of determination (R_z^2) of two groups of parallel velocity distribution data ($z = 12$ mm) is almost equal to 1. The coefficient of determination ($R_\perp^2$) of two groups of perpendicular velocity distribution data ($z = 12$ mm) is 0.9958.

Coefficients of determination (R^2) of four groups of simulation data (emission current density-electric field, spatial distribution, parallel velocity, and perpendicular velocity distribution) are close to 1 based on the two models (dual alloy wires embedded within a rectangular groove and annular surface emitting band). Thus, the annular surface emitting band model can replace the model of dual alloy wires embedded within a rectangular groove to guide the experimental design, although there are minor deviations.

The proposed electron-optical system outlined here is a candidate for use in a 0.6-THz third harmonic TE_{37} mode gyrotron oscillator. According to gyrotron linear theory, the coupling expression depicting the electron beam's interaction with the high-frequency field is given by

$$C_o = \frac{J_{n-s}^2\left(K_{n,p}R_0\right)}{J_n^2\left(\upsilon_{n,p}\right)\left(1 - n^2/\upsilon_{n,p}^2\right)} \tag{2}$$

where s and $\upsilon_{n,p}$ are the pth root of $J_n'(x)$ and the harmonic number, respectively. $k_{n,p} = c_{n,p}/R_0$. R_0 is the guide center radius of the electron beam. In order to increase the coupling coefficient in the 0.6-THz third harmonic gyrotron, $n = s$, ensuring that the $TE_{3\ n}$ mode is selected for higher coupling coefficient. The normalized beam-wave coupling coefficient as a function of beam radius is depicted in Fig. 3.

As shown in Fig. 3, the guiding center radius of the electron beam is 57 μm, and the corresponding normalized coupling coefficient is 0.77. In simulations the 9.2 T superconducting magnetic system has been adopted, with the maximum value of the magnetic field being 7.45 T, and the magnetic field in the emission area is about 2.5 mT. Fig. 4 shows the distribution of the magnetic field along the central axis, and the final design parameters of the CNT cold-cathode electron-optical system are listed in Table I.

The electron beam trajectory is shown in Fig. 5(a). The parallel momentum and perpendicular momentum of the electron beam as a function of axial distance are shown in Fig. 5(b) and (c), respectively. From the simulation results, in Fig. 5, when the electron beam reaches $z = 50$ mm, the parallel momentum of the electron beam gradually decreases. On the contrary, the perpendicular momentum tends to gradually increase, and finally the speed tends to stabilize after the compression stage.

This article has been accepted for inclusion in a future issue of this journal. Content is final as presented, with the exception of pagination.

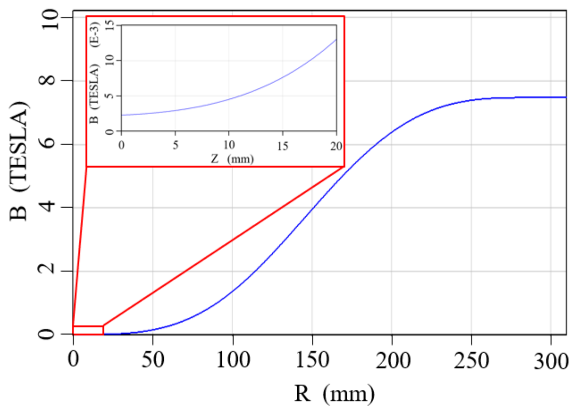

Fig. 4. Profile of the magnetic field intensity along the center axis. Inset: magnetic field intensity local to the cathode.

TABLE I
DESIGN PARAMETERS OF THE ELECTRON-OPTICAL SYSTEM

V_a	Control anode voltage	-22.16 kV
V_b	Accelerating voltage	-23.5 kV
B_c	Magnetic field in cathode area	2.5 mT
B_0	Magnetic field at the output port	7.45 T
R_k	Average radius of emitter	2.74 mm
R_0	Guiding center radius	57 µm
R_L	Larmor radius	51.9 µm
I_b	Beam current	160 mA
J	Emission current density	4.65 A/cm^2
$_z$	Parallel velocity spread	8.9%
$_\perp$	Perpendicular velocity spread	6.7%
$v_\perp/\ v_z$	Velocity ratio	1.1

The perpendicular velocity spread and parallel velocity spread are calculated by

$$\beta_\perp = \frac{v_{\perp\max} - v_{\perp\min}}{v_{\perp\max} + v_{\perp\min}} \tag{3}$$

$$\beta_z = \frac{v_{z\max} - v_{z\min}}{v_{z\max} + v_{z\min}}. \tag{4}$$

The simulation results show that the perpendicular velocity spread and parallel velocity spread of the electron beam are 6.7% and 8.9%, respectively. The velocity ratio of the electron beam is 1.1, and the beam current is 160 mA. These simulation results show that a near-axis small orbit electron beam can be generated by the developed electron-optical system, which makes an important contribution to the control of mode competition in 0.6-THz third harmonic TE_{37} mode gyrotrons.

Design sensitivity to the magnetic field local to the cathode and the control anode voltage have been investigated in Fig. 6(a) and (b), respectively. In Fig. 6(a), the velocity ratio and parallel velocity spread increase as the magnetic field in cathode volume and control anode voltage increase. On the contrary, the perpendicular velocity spread decreases. When the magnetic field in the immediate cathode locality is higher than 6 mT, the parallel velocity spread and the velocity ratio increase rapidly.

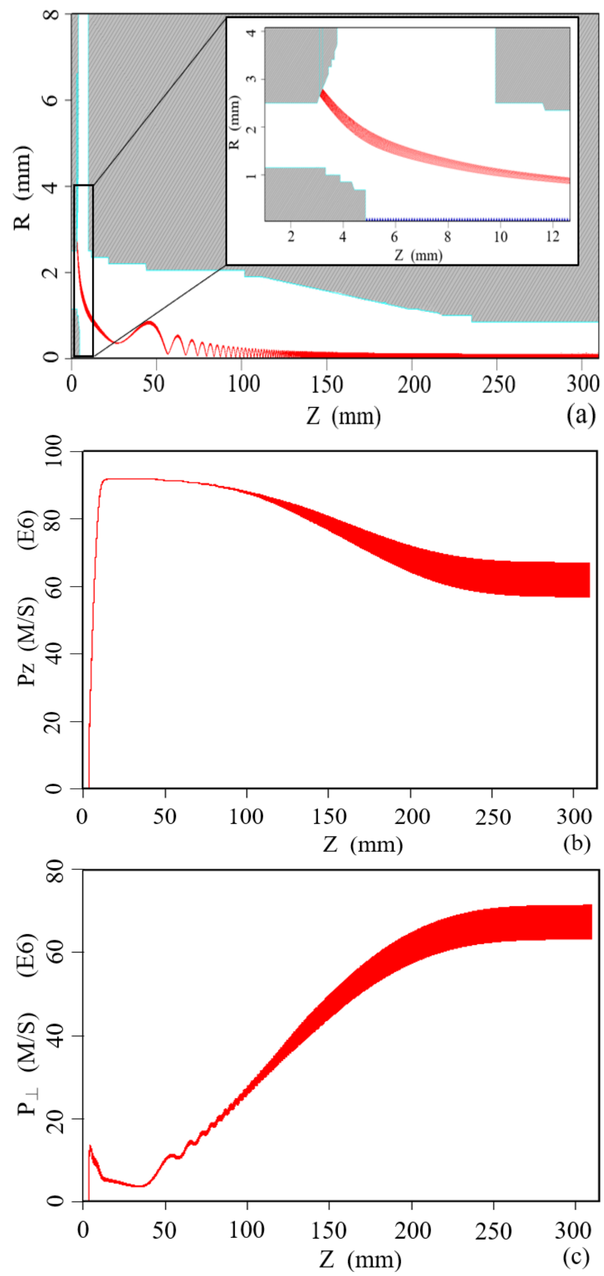

Fig. 5. (a) Electron beam trajectory as a function of axial distance. Inset: detailed view of the electron beam in cathode area. (b) Parallel momenta. (c) Perpendicular momenta as a function of axial distance.

Fig. 6(b) shows that the control anode voltage modulates significantly operation of the electron-optical system. In order to generate the electron beam which can satisfy the necessary high current density in slow wave devices, the velocity ratio and the parallel velocity spread can be decreased as low as 0.44% and 4.7%, respectively, by adjusting control anode voltage. Fig. 7 shows the electron beam trajectory and detailed view of the electron beam at the output port of the electron-optical system (control anode voltage $V_a = -22.36$ kV). The radius of the electron beam is 80 μm. The electron beam current and the emission current density are

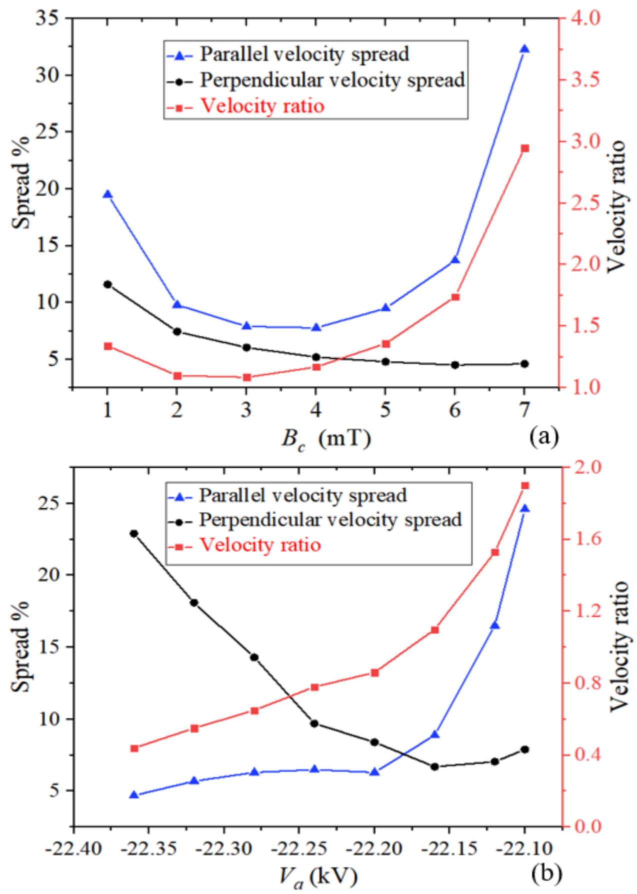

Fig. 6. (a) Design sensitivity to the magnetic field in cathode area. (b) Design sensitivity to the control anode voltage.

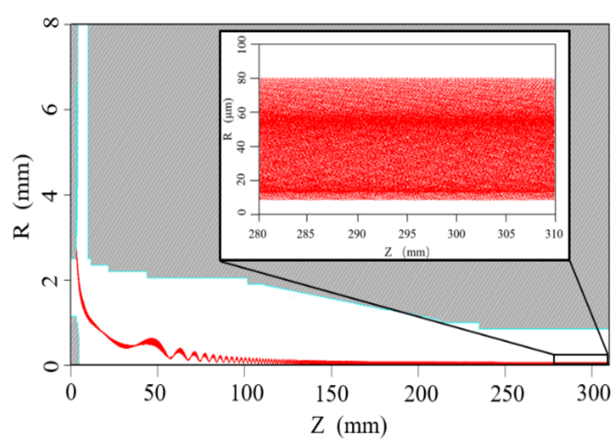

Fig. 7. Electron beam trajectory as a function of axial distance (control anode voltage $V_a = -22.36$ kV). Inset: detailed view of the electron beam at the output port of the electron-optical system.

123 mA and 3.57 A/cm^2, respectively. The parallel energy accounts for 84% of the total energy, and the current density of the electron beam at the output port of the electron-optical system is about 620 A/cm^2, with the electron beam cross-sectional area compressed by 174 times, supporting the generation of the required high beam current densities for terahertz slow wave devices.

III. Conclusion

A high-current-density terahertz electron-optical system, suited for use in fast and slow wave devices, based on a CNT cold cathode has been developed. Mode competition can be well solved by means of the near-axis electron beam in high-order harmonic gyrotrons. Modulation of the control anode voltage has been demonstrated, providing an effective approach to improving the current density. Current density up to 1300 A/cm^2 can be realized if the emission current density increases to the maximum experimental emission current density of 7.65 A/cm^2. The electron-optical system provides a promising perspective for the development of terahertz radiation source based on CNTs and other emerging nanomaterials.

References

[1] J. H. Booske et al., "Vacuum electronic high power terahertz sources," IEEE Trans. THz Sci. Technol., vol. 1, no. 1, pp. 54–75, Sep. 2011, doi: 10.1109/TTHZ.2011.2151610.

[2] R. K. Parker, R. H. Abrams, B. G. Danly, and B. Levush, "Vacuum electronics," IEEE Trans. Microw. Theory Techn., vol. 50, no. 3, pp. 835–845, Mar. 2002, doi: 10.1109/22.989967.

[3] R. J. Barker and E. Schamiloglu, High-Power Microwave Sources and Technologies. Hoboken, NJ, USA: Wiley, 2001.

[4] V. L. Bratman et al., "Gyrotron development for high power THz technologies at IAP RAS," J. Infr., Millim., THz Waves, vol. 33, no. 7, pp. 715–723, Jul. 2012, doi: 10.1007/s10762-012-9898-6.

[5] C. Lei et al., "Analysis of a 0.6-THz second harmonic gyrotron with gradually tapered cavity," IEEE Trans. Plasma Sci., vol. 42, no. 2, pp. 293–299, Feb. 2014, doi: 10.1109/TPS.2013.2295654.

[6] G. S. Nusinovich, M. K. A. Thumm, and M. I. Petelin, "The gyrotron at 50: Historical overview," J. Infr., Millim., THz Waves, vol. 35, no. 4, pp. 325–381, Apr. 2014, doi: 10.1007/s10762-014-0050-7.

[7] G. S. Nusinovich, "Remote detection of concealed radioactive materials by using focused powerful terahertz radiation," J. Infr., Millim., THz Waves, vol. 37, no. 6, pp. 515–535, Jun. 2016, doi: 10.1007/s10762-016-0243-3.

[8] M. Thumm, "Progress in gyrotron development," Fusion Eng. Des., vols. 66–68, pp. 69–90, Sep. 2003, doi: 10.1016/S0920-3796(03)00132-7.

[9] M. K. A. Thumm, "Recent developments on high-power gyrotrons—Introduction to this special issue," J. Infr., Millim., THz Waves, vol. 32, no. 3, pp. 241–252, Mar. 2011, doi: 10.1007/s10762-010-9754-5.

[10] M. Y. Glyavin, N. A. Zavolskiy, A. S. Sedov, and G. S. Nusinovich, "Low-voltage gyrotrons," Phys. Plasmas, vol. 20, no. 3, Mar. 2013, Art. no. 033103, doi: 10.1063/1.4791663.

[11] M. Y. Glyavin, V. N. Manuilov, G. G. Sominskii, E. P. Taradaev, and T. A. Tumareva, "The concept of an electron-optical system with field emitter for a spectroscopic gyrotron," Infr. Phys. Technol., vol. 78, pp. 185–189, Sep. 2016, doi: 10.1016/j.infrared.2016.08.006.

[12] I. V. Bandurkin, V. L. Bratman, Y. K. Kalynov, I. V. Osharin, and A. V. Savilov, "Terahertz large-orbit high-harmonic gyrotrons at IAP RAS: Recent experiments and new designs," IEEE Trans. Electron Devices, vol. 65, no. 6, pp. 2287–2293, Jun. 2018, doi: 10.1109/TED.2018.2797311.

[13] V. L. Bratman, K. Y. Kalynov, and V. N. Manuilov, "Large-orbit gyrotron operation in the terahertz frequency range," Phys. Rev. Lett., vol. 102, no. 24, Jun. 2009, Art. no. 245101, doi: 10.1103/PhysRevLett.102.245101.

[14] X. Yuan, Y. Lan, C. Ma, Y. Han, and Y. Yan, "Theoretical study on a 0.6 THz third harmonic gyrotron," Phys. Plasmas, vol. 18, no. 10, Oct. 2011, Art. no. 103115, doi: 10.1063/1.3647564.

[15] K. Mizuno and S. Ono, "Comment on traveling wave oscillations in the optical region: A theoretical examination," J. Appl. Phys., vol. 46, no. 4, p. 1849, Apr. 1975, doi: 10.1063/1.321757.

[16] S.-T. Han et al., "Experimental investigations on miniaturized high-frequency vacuum electron devices," IEEE Trans. Plasma Sci., vol. 33, no. 2, pp. 679–684, Apr. 2005, doi: 10.1109/TPS.2005.844529.

[17] C. Kory *et al.*, "650 GHz traveling wave tube amplifier," in *Proc. 33rd Int. Conf. Infr., Millim. THz Waves*, Sep. 2008, pp. 1–2, doi: 10.1109/ICIMW.2008.4665623.

[18] Q. Chen, X. Yuan, M. Cole, Y. Zhang, L. Meng, and Y. Yan, "Theoretical study of a 0.22 THz backward wave oscillator based on a dual-gridded, carbon-nanotube cold cathode," *Appl. Sci.*, vol. 8, no. 12, p. 2462, Dec. 2018, doi: 10.3390/app8122462.

[19] X. Yuan *et al.*, "A truncated-cone carbon nanotube cold-cathode electron gun," *Carbon*, vol. 120, pp. 374–379, Aug. 2017, doi: 10.1016/j.carbon.2017.03.046.

[20] X. Yuan *et al.*, "A gridded high-compression-ratio carbon nanotube cold cathode electron gun," *IEEE Electron Device Lett.*, vol. 36, no. 4, pp. 399–401, Apr. 2015, doi: 10.1109/LED.2015.2401593.

[21] K. B. K. Teo *et al.*, "Microwave devices: Carbon nanotubes as cold cathodes," *Nature*, vol. 437, no. 7061, p. 968, Oct. 2005, doi: 10.1038/437968a.

[22] X. Yuan *et al.*, "A fully-sealed carbon-nanotube cold-cathode terahertz gyrotron," *Sci. Rep.*, vol. 6, no. 1, Sep. 2016, Art. no. 32936, doi: 10.1038/srep32936.

[23] H. J. Kim, J. J. Choi, J.-H. Han, J. H. Park, and J.-B. Yoo, "Design and field emission test of carbon nanotube pasted cathodes for traveling-wave tube applications," *IEEE Trans. Electron Devices*, vol. 53, no. 11, pp. 2674–2680, Nov. 2006, doi: 10.1109/TED.2006.884076.

[24] G. Ulisse *et al.*, "Carbon nanotube cathodes for electron gun," *IEEE Electron Device Lett.*, vol. 34, no. 5, pp. 698–700, May 2013, doi: 10.1109/LED.2013.2250247.

[25] G. Ulisse, F. Brunetti, and A. Di Carlo, "Study of the influence of transverse velocity on the design of cold cathode-based electron guns for terahertz devices," *IEEE Trans. Electron Devices*, vol. 58, no. 9, pp. 3200–3204, Sep. 2011, doi: 10.1109/TED.2011.2158437.

[26] Y. Saito and S. Uemura, "Field emission from carbon nanotubes and its application to electron sources," *Carbon*, vol. 38, no. 2, pp. 169–182, 2000, doi: 10.1016/S0008-6223(99)00139-6.

[27] Y. Zu *et al.*, "Design and simulation of a multi-sheet beam terahertz radiation source based on carbon-nanotube cold cathode," *Nanomaterials*, vol. 9, no. 12, p. 1768, Dec. 2019, doi: 10.3390/nano9121768.

[28] W. Lei, Z. Zhu, C. Liu, X. Zhang, B. Wang, and A. Nathan, "High-current field-emission of carbon nanotubes and its application as a fast-imaging X-ray source," *Carbon*, vol. 94, pp. 687–693, Nov. 2015, doi: 10.1016/j.carbon.2015.07.044.

[29] Y. Di *et al.*, "Large and stable emission current from synthesized carbon nanotube/fiber network," *J. Appl. Phys.*, vol. 115, no. 6, Feb. 2014, Art. no. 064305, doi: 10.1063/1.4864431.

[30] X.-L. Yan *et al.*, "Fabrication of carbon nanotube on nickel-chromium alloy wire for high-current field emission," *Appl. Surf. Sci.*, vol. 450, pp. 38–45, Aug. 2018, doi: 10.1016/j.apsusc.2018.04.114.

[31] X. Xu *et al.*, "A low-voltage, premodulation terahertz oscillator based on a carbon nanotube cold cathode," *IEEE Trans. Electron Devices*, vol. 67, no. 3, pp. 1266–1269, Mar. 2020, doi: 10.1109/TED.2020.2968932.